Pakistan Veterinary Journal

ISSN: 0253-8318 (PRINT), 2074-7764 (ONLINE)
DOI: 10.29261/pakvetj/2026.106

RESEARCH ARTICLE

Renoprotective Activity of Fermented *Crescentia cujete* in Rats Subjected to Unilateral Ureteral Obstruction

Yos Adi Prakoso[1], Agustina Dwi Wijayanti[2*], Arifah Binti Abdul Kadir[3], Oscar Maulana Pribadi[1], Sitarina Widyarini[4], Palestin Palestin[5] and Intan Permatasari Hermawan[6]

[1]Department of Pharmacology, Faculty of Veterinary Medicine, University of Wijaya Kusuma Surabaya, East Java, 60225, Indonesia; [2]Department of Pharmacology, Faculty of Veterinary Medicine, Universitas Gadjah Mada, Yogyakarta, 55281, Indonesia; [3]Faculty of Veterinary Medicine, Universiti Putra Malaysia, Selangor, 43400, Malaysia; [4]Department of Pathology, Faculty of Veterinary Medicine, Universitas Gadjah Mada, Yogyakarta, 55281, Indonesia; [5]Department of Clinical Pathology, Faculty of Veterinary Medicine, University of Wijaya Kusuma Surabaya, East Java, 60225, Indonesia; [6]Department of Internal Medicine, Faculty of Veterinary Medicine, University of Wijaya Kusuma Surabaya, East Java, 60225, Indonesia
*Corresponding author: wagustinadwi@gmail.com

ARTICLE HISTORY (26-012)

Received: January 08, 2026
Revised: March 25, 2026
Accepted: April 07, 2026
Published online: April 12, 2026

Key words:
Clinicopathology
Fermented *Crescentia cujete*
Hydronephrosis
Rats
Renoprotective activity
Unilateral ureteral obstruction

ABSTRACT

Unilateral ureteral obstruction (UUO) induces hydronephrosis in the affected kidney, with compensatory damages in the contralateral kidney. This study aimed to evaluate the renoprotective effects of fermented *Crescentia cujete* (FCC) on the contralateral kidney in UUO-induced rats. Based on a preliminary study, 14 days post-UUO-induction (dpi) was selected as the treatment baseline for initiating treatments. For the main study, 24 six-month-old male rats (weighing 315.05±3.22g) were subjected to right UUO and randomly assigned to three groups: G1 (sham-operated), G2 (untreated UUO), and G3 (UUO treated with 11.84mg/kg FCC). From 15 to 28 dpi, group G3 rats received oral FCC twice daily, while those of G1 and G2 remained untreated. On 29 dpi, rats were evaluated for lower limb oedema, blood pressure, SDMA, cystatin C, creatinine clearance and renal ultrasonography; and kidney macroscopy, histopathology for tubular injury, inflammation and fibrosis, and immunohistochemical expression of claudin-1, NGAL, SPP1, TNF-α following euthanasia. Results showed that right kidneys in groups G2 and G3 exhibited higher hydronephrosis, tubular injury, inflammation, and fibrosis scores compared to G1 ($P<0.05$), with no differences between G2 and G3. In the contralateral kidney, FCC improved length, width, thickness, volume, weight of kidney, hydronephrosis scores, and histopathological lesions compared to G2 ($P<0.05$), with non-significant differences in these parameters between rats of groups G1 and G3. Systemically, FCC reduced lower limb oedema, blood pressure, SDMA, and elevated creatinine clearance compared to UUO+FCC ($P<0.05$). Moreover, FCC downregulated the immunoexpression of NGAL, SPP1, and TNF-α in the contralateral kidney ($P<0.05$). FCC treatment also restored cystatin C level to sham-treated control group. In conclusion, FCC demonstrated renoprotective effects in the contralateral kidney of UUO rats by preserving renal morphology and suppressing pro-inflammatory and pro-fibrotic markers.

To Cite This Article: Prakoso YA, Wijayanti AD, Kadir ABA, Pribadi OM, Widyarini S, Palestin P and Hermawan IP, 2026. Renoprotective activity of fermented *Crescentia cujete* in rats subjected to unilateral ureteral obstruction. Pak Vet J, 46(5): 1187-1196. http://dx.doi.org/10.29261/pakvetj/2026.106

INTRODUCTION

The kidney is a vital body organ responsible for eliminating waste products, filter blood and reabsorb essential metabolites. Both the left and right kidneys work together in a coordinated, harmonious manner, so impairment of one kidney or ureter often leads to compensatory changes in the contralateral normal kidney or ureter. Ureteral obstruction is a common renal disorder, which can arise from blood clots, mineral deposits, tumours, or other abnormalities of the urinary tract (Ilgi *et al.,* 2020). This blockage causes urine to reflux, leading to

the progressive development of hydronephrosis (Arifianto *et al.,* 2020).

Hydronephrosis caused due to unilateral ureteral obstruction (UUO) is usually characterized by glomerular atrophy, tubular-cystic transformation, inflammation, and fibrosis (Damian *et al.,* 2022). Rise in intrarenal pressure has adverse effects on nephrons and impairs their integrity, structure, and function (Hosny *et al.,* 2024). Unilateral ureteral obstruction can also induce various compensatory changes in the contralateral normal kidney, such as inflammation, necrosis, and mild to severe tubular dilation (Isac and Ionescu, 2025).

In standard clinical practice, diuretics such as furosemide are routinely administered to UUO patients for reducing intraluminal pressure in the contralateral normal kidney (Pokrovskaya *et al.,* 2021). Furosemide can be used to facilitate the diagnosis (Bombiński *et al.,* 2018) and management of mild hydronephrosis (Patel *et al.,* 2014). However, the efficacy of furosemide decreases in severe hydronephrosis (Dilken *et al.,* 2023). Hence, the alternative therapies need to be developed for managing the entire range of hydronephrosis severity. Fermented *Crescentia cujete* (FCC) has been shown to be a promising candidate for managing such problem (Prakoso *et al.,* 2025).

The FCC contains high levels of choline, which is essential for neurology (Hidayah *et al*., 2023) and normal kidney function (Kenny *et al.,* 2025). Choline is a fundamental compound related to the phospholipid group and required to maintain nephron structure (Liu *et al.,* 2025). A recent study by Dias *et al.* (2023) has indicated that natural phosphatidylcholine showed high bioavailability for kidney tissue repair. According to Wijayanti *et al.* (2024), FCC enhances immune function by elevating plasma antioxidant levels in animal models, which potentially protects the kidney from oxidative damage during hydronephrotic stress.

Due to its high choline level, the use of FCC is expected to promote the nephron integrity in hydronephrosis (Kenny *et al.,* 2025). The FCC is also postulated to prevent further compensatory impacts (Li *et al.,* 2024) and enhance diuresis which is crucial in lowering intraluminal pressure (He *et al.,* 2022). Therefore, the present study was planned to evaluate the renoprotective activity of fermented *Crescentia cujete* on the contralateral normal kidney in rats subjected to unilateral ureteral obstruction.

MATERIALS AND METHODS

Fermentation and choline standardization of *Crescentia cujete*: *Crescentia cujete* fruit were collected from the University of Wijaya Kusuma Surabaya, Indonesia and fermented following the procedure described by Wilujeng *et al.* (2023). Briefly, the fruit was peeled, and 400g of pulp was diluted with 1000mL of distilled water. The mixture was stirred and homogenized. Moreover, 40mL of pectinase and 40g of granulated white cane sugar (Gulaku®, Indonesia) were added to the mixture. The mixture was stored at room temperature for 30 days with daily stirring. On day 31, the filtrate was collected and stored in a refrigerator until use.

The choline contents of FCC were standardized using LC-MS/MS method described earlier (Prakoso *et al.*, 2024). For this purpose, 10mg of FCC was mixed with 200µL of 50mM hydrochloric acid. The mixture was then homogenized. The supernatant was diluted 100-fold using a mobile phase containing 0.01% formic acid in 50% methanol. The analysis was performed using a SCIEX Triple Quad 5500+LC-MS/MS system. The monitored choline transition was at a mass/charge ratio (m/z) of 104.2 to 60.2. Choline standard solutions were prepared in the mobile phase at concentrations ranging from 0 to 24mg/kg. The calibration curve exhibited a linear regression equation of $y=3.15\times10^5x+2.0\times10^4$, where y is the analyte peak area, x is the choline concentration in mg/kg, with an $R2$ value of 0.998. This procedure was performed in triplicate. The choline concentration in FCC was found to be 115.25±4.33mg/mL.

Preliminary study: Induction of unilateral ureteral obstruction: For preliminary study, four male Sprague Dawley rats (aged six months and weighing 305.18±4.87g) were anesthetized using xylazine (4mg/kg BW; Ilium, Australia) and Zoletil® (30mg/kg BW; Virbac, India), intramuscularly. The abdominal area was disinfected with 70% isopropyl alcohol. The skin was incised, and the intestines and mesentery were retracted. Middle segment of the right ureter was ligated with a simple interrupted 4-0 nylon suture (Ailee, Korea). The intestines were repositioned and 20mg/kg BW enrofloxacin was applied. The abdominal wall and skin were closed with simple interrupted 2-0 catgut and 2-0 braided silk sutures, respectively.

At 14 days post-induction (dpi), ultrasonography revealed remarkable swelling and hydronephrosis in the right kidney (width, 16.52mm; length, 25.85mm) compared to the left kidney (width, 8.60mm; length, 13.37mm; Fig. 1A). Macroscopic examination at euthanasia confirmed that right kidney (width, 21.11mm, length, 25.48mm, volume, 4.741mm^3, and weight, 4.35g) was enlarged compared to the left kidney (width, 11.05mm, length, 19.17mm, volume, 1.121mm^3, and weight, 0.89g; Fig. 1B). Serum creatinine level reached 1.23±0.08mg/dL (exceeding the normal range of 0.4–0.8mg/dL). Based on these results, 14 days post-UUO induction was selected as the baseline for initiating FCC treatment.

Research design: A total of 24 adult male Sprague Dawley rats, aged 6 months with body weight of 315.05±3.22g, were housed individually in metabolic cages (50×30×40cm) and given feed and water *ad libitum*. The room temperature was maintained at 25°C, with 65% humidity, and rice husk was used as bedding. The rats were randomly assigned to three groups, with 8 rats in each group: G1 (sham-operated), G2 (UUO without FCC treatment), G3 (UUO+11.84mg/kg FCC dose based on Hidayah *et al.,* 2023). Unilateral right-sided ureter obstruction (UUO) was induced in rats of all three groups, as described under preliminary study. Starting on 15 dpi, rats in G3 group received FCC (11.84mg/kg) by oral gavage twice daily for 14 days, while rats of groups G1 and G2 received no treatment for 28 days after UUO induction.

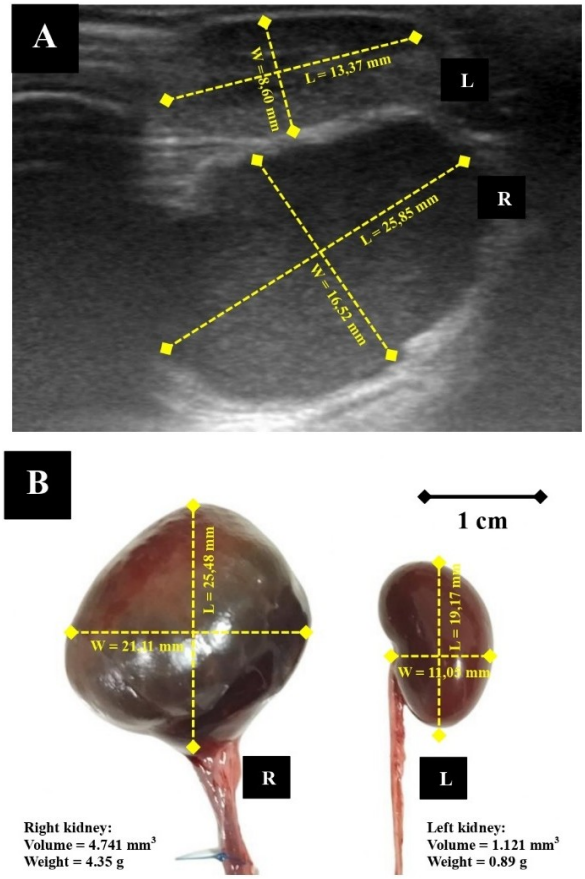

Fig. 1: Ultrasonographic and macroscopic appearance of rat kidneys 14 days after induction of UUO (preliminary study). (A): Ultrasonographic images reveal dilation of the renal pelvis (width=16.52mm, length=25.85 mm) in the right kidney (R), appearing as a large anechoic area, while the left kidney (L) shows a normal renal pelvis (width=8.60mm, length=13.37mm). (B): Gross examination shows an enlarged right kidney (R) with disrupted architecture, whereas the left kidney (L) shows normal appearance.

Oedema scoring of the lower-limbs: Lower-limb oedema was evaluated at 29 dpi in rats of all three experimental groups. Oedema severity was scored on a scale of 0 to 4 (Table 1), as described previously (Gasparis *et al.,* 2020).

Table 1: Scoring system of the lower limb oedema of experimental rats

Parameters	Oedema score				
	0	1	2	3	4
Visual swelling	No swelling	Mild swelling, barely noticeable	Minimal swelling, easily visible	Moderate swelling, significantly enlarged limb	Severe swelling, possibly with skin changes or ulceration
Pitting oedema	No pitting oedema	The indentation immediately rebounds	The indentation rebounds within 15sec	The indentation rebounds within 16-30sec	The indentation rebounds >30sec
Mid tibia circumference (cm)	Direct measurement using gauge				
Ankle circumference (cm)	Direct measurement using gauge				
Swelling position	No swelling	Unilateral	Bilateral	-	-

Source: Gasparis *et al.* (2020)

Blood pressure analysis: Blood pressure was measured using a tail-cuff system on 29 dpi. The systolic, diastolic, and mean arterial pressures were recorded using a Contec08A-VET blood pressure monitor (Contec, China).

Renal ultrasonography: On day 29 post UUO induction, the rats were sedated with xylazine (4mg/kg BW). Then the rats were restrained, their backs were shaved, and both kidneys were assessed for hydronephrosis using an ultrasonography unit equipped with a linear-array transducer and operating at 6.5–9.4MHz frequency (Edan DUS60, China). In this way, renal length and cortical thickness were measured.

Hydronephrosis scoring was performed on the ipsilateral and contralateral kidneys. The scale was defined as follows: 0=no hydronephrosis/normal kidney appearance; 1=dilation of the renal pelvis with normal cortex; 2=moderate renal pelvis dilation with minimal cortical thinning; 3=marked renal pelvis dilation with moderate cortical thinning; and 4=severe renal pelvis dilation with pronounced cortical thinning, as described previously (Vilskersts *et al.*, 2020).

Clinicopathological analysis: Rat blood was collected via the retroorbital plexus under anaesthesia on day 29 of UUO induction. The blood was collected in EDTA and plain tubes. The samples were centrifuged to separate the plasma and serum, respectively. Urine was also collected on 29 dpi using cystocentesis. The plasma, serum and urine samples were stored at 4°C prior to analysis. Serum symmetric dimethylarginine (SDMA) and cystatin C were determined by ELISA using the SDMA ELISA kit (ab213973, Abcam, UK) and the cystatin C ELISA kit (BMS2279, Invitrogen, USA), respectively. Plasma and urine creatinine levels were measured with a creatinine assay kit (MAK080, Sigma-Aldrich, USA). Measurements of SDMA, cystatin C and creatinine were conducted following the instructions given with the relevant kit. The creatinine clearance was calculated using the equation: Creatinine clearance=(CU × UF)/ CP, where CU is urine creatinine concentration, UF is urine flow rate per hour and CP is plasma creatinine concentration (Chen and Chiaramonte, 2019).

Renal macroscopy and histopathology: The rats from all group were euthanized with 150 mg/kg BW ketamine on day 29 of UUO induction. Kidneys were then harvested and their length, width, thickness, volume, and weight were measured. Kidney sections were fixed in 10% neutral buffered formalin (NBF), and processed for routine histopathology using H&E staining (Ma *et al.,* 2024). A pathologist scored histopathological changes using a semi-quantitative scale 1 to 5: 1=normal/no change; 2=mild (>1-25% tissue changed); 3=minimal (>25-50% tissue changed); 4=moderate (>50-75% tissue changed); 5=severe (>75% tissue changed), as described earlier (Vilskersts *et al.,* 2020). Assessed parameters included tubular injury, inflammation, and fibrosis.

Renal immunohistochemistry: The kidney tissue was also processed for immunohistochemistry (IHC) against anti-claudin-1 (sc-166338, Santa Cruz Biotechnology, USA), anti-NGAL (ABS 043-29-2, Invitrogen, USA), anti-SPP1

(CSB-RA261140A0HU, Cusabio Technology LLC, USA), and anti-TNF-α (PA5-19810, Invitrogen, USA). Antibody dilutions were 1:250 for claudin-1 and NGAL, 1:100 for SPP1, and 1:150 for TNF-α. The incubation times were 60min for claudin-1, 30min for NGAL and SPP1, and overnight for TNF-α. The immunohistochemistry was performed following the manufacturer's instructions. The IHC slides were analyzed using ImageJ to determine the percentage of immunoreactive area.

Statistical analysis: Data of lower-limb oedema scores, ultrasonography scores, and histopathological scores were analyzed using Kruskal–Wallis and Mann–Whitney U tests. The remaining data were subjected to one-way ANOVA, followed by Duncan's multiple range test. A 95% confidence level (P<0.05) was applied throughout the analysis.

RESULTS

Oedema scoring of the lower-limbs: Oedema scoring revealed that rats of group G2 (UUO treated) exhibited significantly higher oedema scores than those of groups G1 (control) and G3 (UUO+FCC treated) for visual swelling, pitting oedema, mid-tibia and ankle circumferences, and swelling location (P<0.05). However, group G3 did not differ significantly from G1 in these parameters (Table 2). Gross morphological changes in hind limbs for rats of groups G1, G2 and G3 are shown in Figs. 2A, 2B and 2C, respectively.

Blood pressure: The systolic (Fig. 2D), diastolic (Fig. 2E), and mean arterial blood pressures (Fig. 2F) in rats of group G2 were significantly higher than rats in groups G1 and G3 (P<0.05). However, the differences in systolic and mean arterial pressures between rats of groups G1 and G3 were non-significant. Moreover, FCC treatment (group G3) significantly reduced diastolic blood pressure compared to group G2, although it remained higher than that in group G1 (P<0.05).

Table 2: Lower-limb oedema scores and other related parameters in rats of different experimental groups

Parameters	Experimental groups		
	G1 (Control)	G2 (UUO)	G3 (UUO+FCC)
Visual swelling (score)	0.00±0.00^a	3.75±0.50^b	0.25±0.50^a
Pitting oedema (score)	0.00±0.00^a	2.75±0.50^b	0.25±0.50^a
Mid tibia circumference (cm)	5.82±0.20^a	10.80±0.65^b	6.83±1.60^a
Ankle circumference (cm)	3.65±0.25^a	5.61±0.42^b	3.80±0.32^a
Swelling position	0.00±0.00^a	1.75±0.50^b	0.25±0.50^a

Values with different superscripts in the same row show statistically significant differences (P<0.05).

Renal echotexture: Ultrasonographic examination of kidneys showed that rats in groups G2 and G3 exhibited significantly higher hydronephrosis scores for the right kidney than those in group G1 (P<0.05). Hydronephrosis in the right kidney caused by UUO remained unresolved after FCC treatment, as evidenced by non-significant difference in ultrasonographic scores between groups G2 and G3 (Table 3). In contrast, ultrasonographic scores for the left kidney showed that group G2 had significantly higher values than groups G1 and G3 (P<0.05), while non-significant difference was observed between groups G1 and G3 (Table 3).

Table 3: Ultrasonographic hydronephrosis scores in rat kidneys of different experimental groups

Side of the Kidney	Experimental groups		
	G1 (Control)	G2 (UUO)	G3 (UUO+FCC)
Right kidney	0.00±0.00^a	3.75±0.50^b	3.50±0.57^b
Left kidney	0.00±0.00^a	1.25±0.50^b	0.25±0.50^a

Values with different superscripts in the same row show statistically significant differences (P<0.05).

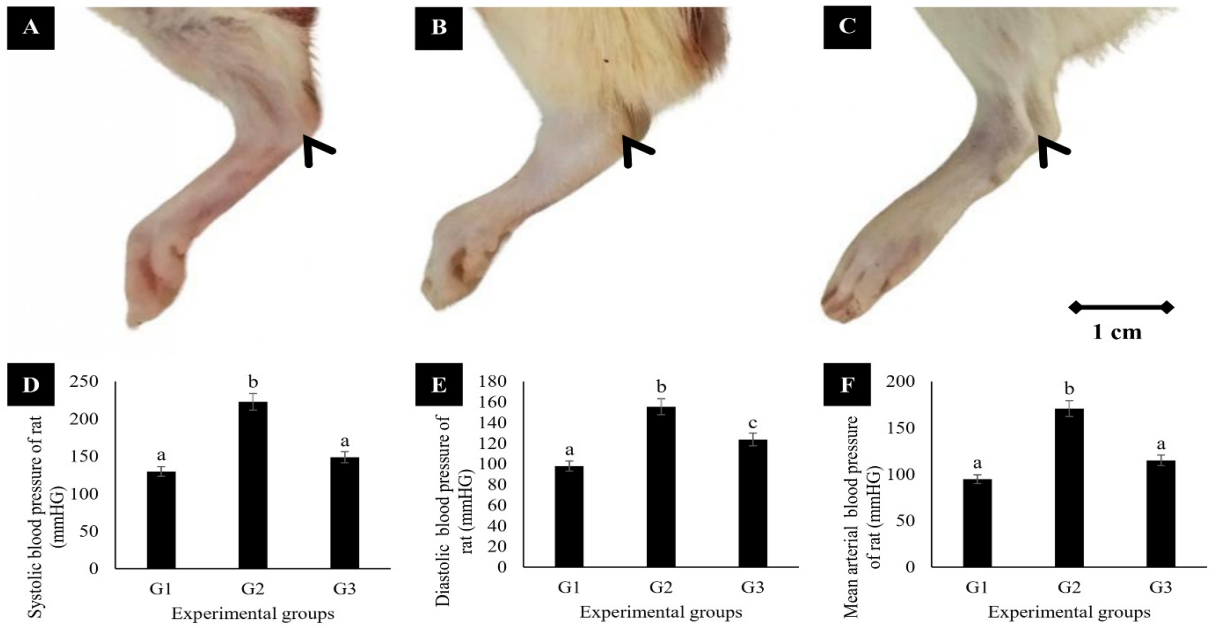

Fig. 2: Gross morphology of rat hind limbs and blood pressure of different experimental groups. (A): Sham-operated control rats (G1) displaying the left hind limb with a normal (arrowhead) appearance. (B): Untreated UUO rats (G2) showing pronounced swelling and oedema in the left hind limb (arrowhead). (C): FCC-treated UUO rats (G3) exhibiting minimal swelling in the left hind limb (arrowhead). (D): Systolic; (E): Diastolic; and (F): Mean arterial blood pressure in UUO rats. Scale bar: 1cm (A-C). Bars with different letters for each parameter denote statistically significant differences (P<0.05).

Ultrasonographs showing the length and width of right and left kidneys of rats from groups G1, G2 and G3 are shown in Figs. 3A, 3B and 3C, respectively. Ultrasonographic assessment of renal length showed that right kidney in groups G2 and G3 was significantly longer than in group G1 (P<0.05). The difference in right kidney length between rats of groups G2 and G3 was non-significant. Furthermore, cortical thickness of the right kidney in groups G2 and G3 could not be measured due to marked cortical thinning (Fig. 3D). For the left kidney, rats of G2 group exhibited significantly higher length compared with G1 and G3 groups (P<0.05), the differences in left kidney length between rats of latter two groups were non-significant. The cortical thickness did not differ among rats of three groups (Fig. 3D).

Serum biomarkers and creatinine clearance: In the present study, UUO induced a significant increase in SDMA and cystatin C levels compared to control group (P<0.05), with SDMA increasing 1.5-fold (Table 4). After FCC treatment, SDMA in G3 remained elevated compared to G1 but was lower than in G2 (P<0.05). Cystatin C levels in G3 differed non-significantly from those in G1. Creatinine clearance dropped in G2 following UUO compared with G1 (P<0.05). FCC administration in G3 resulted in a partial recovery of creatinine clearance relative to G2 (P<0.05), although values remained below those of G1 (P<0.05; Table 4).

Renal macroscopy: Following euthanasia, gross morphology of the right kidney in groups G2 and G3 revealed enlargement compared to G1 (P<0.05). Although the right kidney was smaller in group G3 than in G2, particularly in length, width, volume, and weight (P<0.05), its thickness did not differ between G2 and G3 groups. Furthermore, the right kidney in G3 remained enlarged than that in G1 in terms of length, width, thickness, volume and weight (P<0.05; Table 5).

Table 4: Symmetric dimethylarginine (SDMA), cystatin C and creatinine clearance in rats of three experimental groups

Parameters	Experimental groups		
	G1 (Control)	G2 (UUO)	G3 (UUO+FCC)
SDMA (ug/dL)	8.45±0.50[a]	12.84±1.08[b]	10.05±0.57[c]
Cystatin C (ng/mL)	1440.47±60.82[a]	2186.35±331.79[b]	1390.11±132.85[a]
Creatinine clearance (mL/min)	7.46±1.50[a]	0.29±0.11[b]	2.54±0.90[c]

Values with different superscripts in the same row show statistically significant differences (P<0.05).

Table 5: Macroscopic evaluation of kidneys in rats of three experimental groups following euthanasia

Parameters		Experimental groups		
		G1 (Control)	G2 (UUO)	G3 (UUO+FCC)
Right kidney	Length (mm)	13.81±0.41[a]	26.87±1.92[b]	23.20±0.99[c]
	Width (mm)	9.22±0.35[a]	20.87±3.31[b]	16.60±1.36[c]
	Thickness (mm)	7.16±0.21[a]	15.80±3.42[b]	14.15±0.86[b]
	Volume (mm^3)	477.54±33.82[a]	4654.53±1346.66[b]	2875.30±514.55[c]
	Weight (g)	0.63±0.09[a]	4.53±0.78[b]	3.19±0.34[c]
Left kidney	Length (mm)	13.03±0.54[a]	19.17±1.66[b]	15.23±1.65[a]
	Width (mm)	9.01±0.25[a]	10.59±1.71[b]	8.50±0.47[a]
	Thickness (mm)	8.23±0.31[a]	10.21±1.29[b]	8.25±0.16[a]
	Volume (mm^3)	505.66±30.16[a]	1,100.46±312.83[b]	558.86±67.86[a]
	Weight (g)	0.65±0.07[a]	0.84±0.05[b]	0.58±0.04[a]

Values with different superscripts in the same row show statistically significant differences (P<0.05).

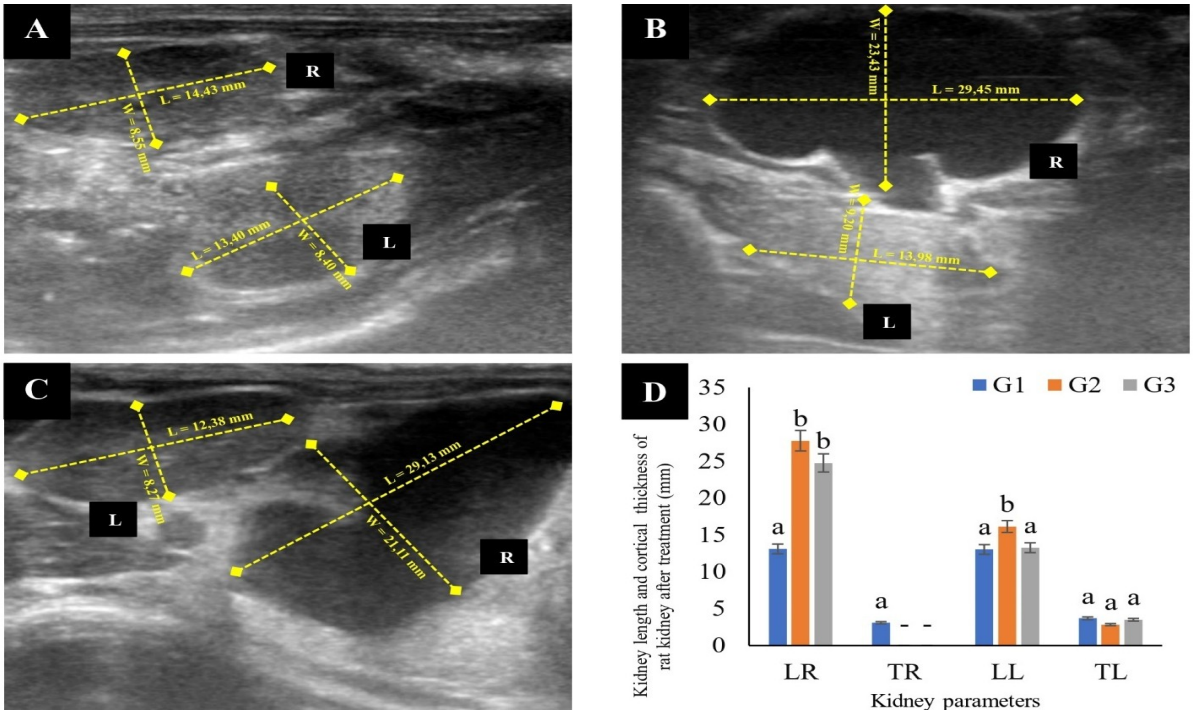

Fig. 3: Ultrasonographic morphology of rat kidneys of different experimental groups. (A): Sham-operated control (G1), displaying normal renal morphology with comparable dimensions of the left (L) and right (R) kidneys. (B): UUO treated rats (G2), showing an enlarged anechoic area in the right kidney (R) and suspected enlargement of the left kidney (L). (C): UUO+FCC-treated rats (G3), demonstrating similar feature of the right kidney (R) with G2 group and clear visualization of the renal pelvis in the left kidney (L). (D): Quantitative ultrasonographic comparison of renal length and cortical thickness across G1, G2, and G3. LR=right kidney length; TR=cortical thickness of the right kidney; LL=left kidney length; TL=cortical thickness of the left kidney; (-) =unmeasurable using USG. Bars with different letters for the same parameter denote statistically significant differences (P<0.05).

Gross examination of the left kidney in UUO rats without FCC treatment (G2) demonstrated a compensatory increase in length, width, thickness, volume, and weight compared to G1 (P<0.05). In contrast, left kidney measurements in rats of G3 were comparable to those of G1, although these measurements were significantly lower than those of G2 (P<0.05; Table 5).

Renal histopathology: Histopathological examination of kidneys showed that tubular injury, inflammation, and fibrosis scores of the right kidney were significantly higher in groups G2 and G3 than in G1 (P<0.05). However, non-significant differences were observed in these parameters of the right kidney between the former two groups (Table 6). The qualitative histopathological findings of the right kidneys are shown in Fig. 4A-D. The right kidney in G1 group indicated intact glomeruli and tubules (Fig. 4A). However, G2 group showed tubular atrophy and tubule-cystic degeneration, accompanied by inflammation and fibrosis (Fig. 4B). Tubuloepithelial depletion and transitioning from cuboid to squamous epithelium was also observed in G2 rats (Fig. 4C). G3 group indicated severe necrosis and extensive fibrosis (Fig. 4D).

Histopathological analysis of the left kidney revealed no histopathological changes in G1 group (Fig. 4E). In contrast, the UUO untreated G2 group exhibited tubular vacuolization, interstitial fibrosis, inflammation and severe tubular necrosis (Fig. 4F-H). The UUO+FCC-treated G3 group exhibited mild inflammation and tubular vacuolization (Fig. 4I & 4J). Statistically, histopathological scores for rats of group G2 were significantly higher compared to those of G1 and G3 (P<0.05). Interestingly, the UUO+FCC-treated G3 group did not differ from the sham-operated G1 group in terms of tubular injury, inflammation, or fibrosis (Table 6).

Table 6: Histopathological scores of kidneys in rats of three experimental groups following euthanasia

Parameters		Experimental groups		
		G1 (Control)	G2 (UUO)	G3 (UUO+FCC)
Right kidney	Tubular injury	1.00±0.00^{a}	4.50±0.57^{b}	4.50±0.57^{b}
	Inflammation	1.00±0.00^{a}	3.75±0.95^{b}	4.00±0.81^{b}
	Fibrosis	1.00±0.00^{a}	3.75±0.95^{b}	3.25±0.50^{b}
Left kidney	Tubular injury	1.00±0.00^{a}	4.50±0.57^{b}	1.50±0.57^{a}
	Inflammation	1.00±0.00^{a}	3.25±0.50^{b}	1.50±0.57^{a}
	Fibrosis	1.00±0.00^{a}	3.25±0.50^{b}	1.25±0.50^{a}

Values with different superscripts in the same row show statistically significant differences (P<0.05)

Renal immunohistochemistry: Renal immunohistochemistry of the left kidney showed that claudin-1 was localized in the Bowman's capsule and along the distal convoluted tubules (Fig. 5A). The NGAL was detected in the renal tubular epithelium and infiltrating inflammatory cells (Fig. 5B). Immunoreactivity for SPP1 (Fig. 5C) and TNF-α (Fig. 5D) also appeared in the renal tubules.

For the left kidney of UUO treated rats, groups G2 and G3 exhibited higher immuno-expression levels of claudin-1 than that of group G1 (P<0.05); the difference between the former two groups was non-significant (Fig. 5E). Significantly elevated immuno-expression levels of NGAL (Fig. 5F), SPP1 (Fig. 5G), and TNF-α (Fig. 5H) were recorded in group G2 compared to groups G1 and G3 (P<0.05). Moreover, G3 displayed significantly reduced immunoreactivity for NGAL, SPP1, and TNF-α relative to G2 (P<0.05), although levels of claudin-1, NGAL, SPP1, and TNF-α remained significantly higher than those in G1 (P<0.05).

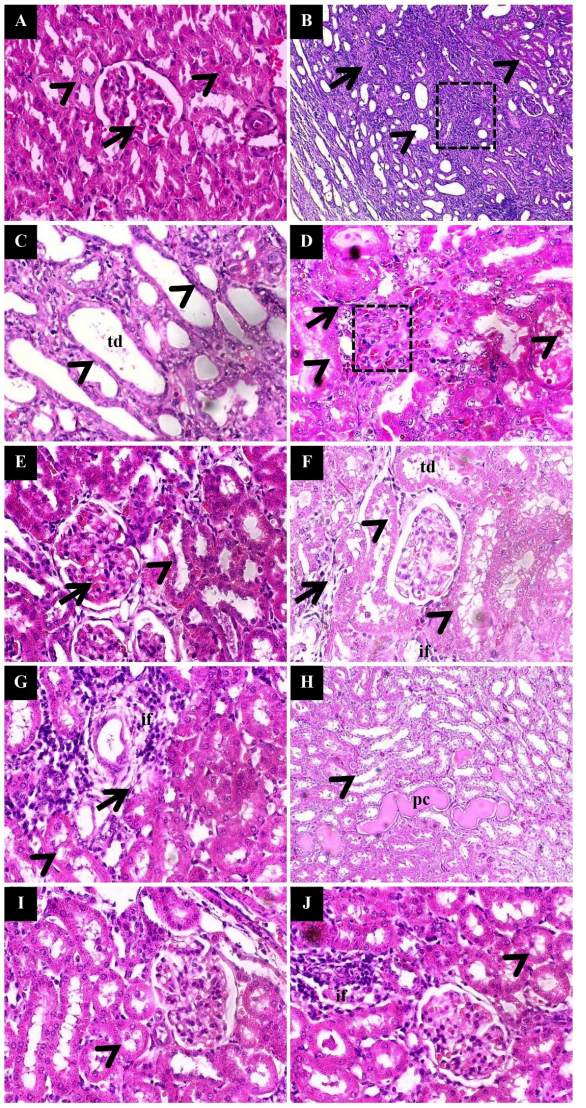

Fig. 4: Histopathological examination of right (A–D) and left (E–J) kidneys in rats of three groups. Right kidneys: (A): Sham-operated control group (G1) shows normal renal architecture with intact glomeruli (arrow) and tubules (arrowhead). (B): Untreated UUO rats (G2) exhibiting pronounced tubulo-cystic degeneration, tubular atrophy (arrowhead), lymphocytic interstitial inflammation (boxed), and interstitial fibrosis (arrow). (C): G2 group also exhibiting tubuloepithelial depletion (arrowhead) and widening of renal tubules (td) with cuboidal epithelium transitioning to squamous epithelium. (D): UUO+FCC-treated rats (G3) showing severe glomerular necrosis (boxed) replaced by fibroblasts (arrow) and tubular necrosis with epithelial disruption (arrowhead). Left kidneys: (E): Sham-operated control (G1) shows normal renal architecture with intact glomeruli (arrow) and tubules (arrowhead). (F, G): Untreated UUO rats (G2) showing interstitial fibrosis (arrow), inflammatory cell infiltration (if), tubular vacuolization (arrowhead), dilatation (td). (H): G2 group also indicating moderate tubular necrosis (arrowhead) with intratubular eosinophilic masses suspected to be protein casts (pc). (I): FCC-treated UUO rats (G3) show mild tubular epithelial vacuolization (arrowhead). (J): G3 kidney further exhibits focal interstitial inflammation (if). H&E staining; magnifications: 100× (B, H), 400× (A, C, D–G, I, J).

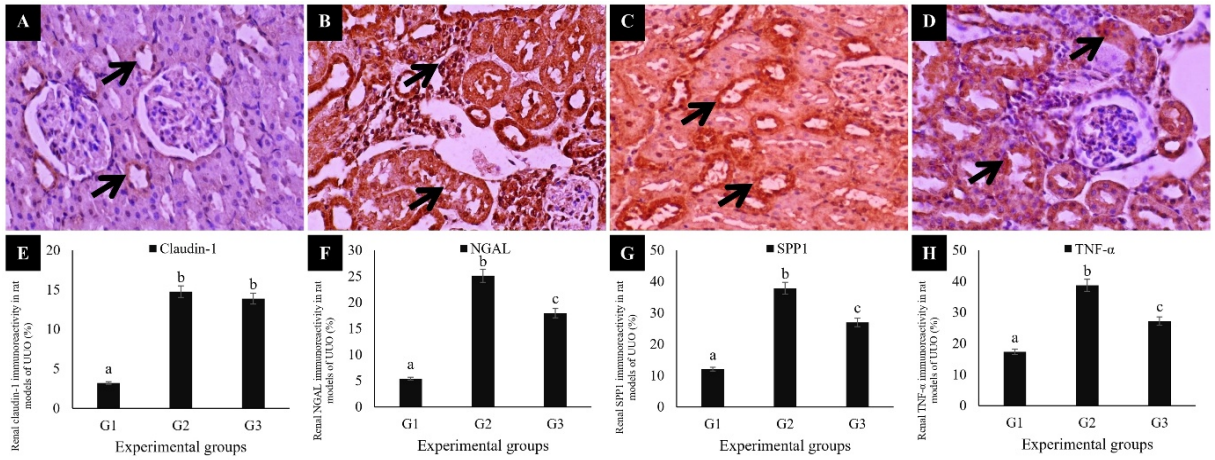

Fig. 5: Immunohistochemical examination of claudin-1, NGAL, SPP1, and TNF-α in the left kidney of rats of different groups (A): Claudin-1 immunoreactivity is localized in the renal tubules and Bowman's capsule (arrow). (B): NGAL staining is detected in infiltrating inflammatory cells and tubular epithelium (arrow). (C): SPP1 expression is confined to the thick ascending limb and distal convoluted tubules (arrow). (D): TNF-α immunoreactivity is observed in tubular cells (arrow). (E–H): Quantification of the percentage of immunoreactivity area for claudin-1 (E), NGAL (F), SPP1 (G), and TNF-α (H) in rat kidneys. IHC staining; antibody anti-claudin-1 (A), anti-NGAL (B), anti-SPP1 (C), and anti-TNF-α (D); magnifications: 400× (A-D); DAB chromogen.

DISCUSSION

Unilateral ureteral obstruction (UUO) is a common cause of hydronephrosis, leading to progressive dilation of the renal pelvis and calyces on the affected side. As intraluminal pressure rises, tubular epithelial cells are damaged due to necrosis, and glomeruli undergo atrophy (Napitupulu *et al.,* 2023). Prostaglandin-mediated signaling is one of the first ways the body tries to overcome this increased intraluminal pressure. In the first mechanism, the thromboxane A_2 and angiotensin II cause narrowing of the afferent arteriole and the efferent arteriole concomitantly (Kobori *et al.,* 2013). These hemodynamic changes work synergistically to reduce the glomerular filtration rate (GFR; Pérez-Aizpurua *et al.,* 2024).

Histopathologically, prolonged ischemia stimulates the release of danger-associated molecular patterns (DAMPs) from necrotic nephron cells. These DAMPs increase the level of SPP1, which then stimulates the macrophages and neutrophils to release NGAL and TNF-α (Shi and Zhu, 2023). Excessive expression of these mediators further worsens tubular atrophy and apoptosis and stimulates claudin-1 expression (Iida *et al.,* 2022). Abnormal distribution of Claudin-1 disrupts the structure and function of blood vessels and tubules. In advanced stages, increased macrophage infiltration stimulates myofibroblasts, leading to extracellular matrix deposition in the interstitium and resulting in fibrosis (Jo *et al.,* 2022). These alterations on the ipsilateral side of UUO decrease GFR, lower the creatinine clearance, and gradually increase SDMA and cystatin C levels (Benoit *et al.,* 2020).

The histopathological alterations in the UUO affected kidney cannot be reversed due to sustained high intraluminal pressure, unless the underlying obstruction is resolved (Yaxley and Yaxley, 2023). Results of the present study consistently showed non-significant changes between the UUO-affected right kidneys with FCC treatment (group G3) or without FCC treatment (group G2), regarding tubular injury, inflammation and fibrosis. Ipsilateral kidney of rats of these both groups (G2 and G3) also showed similar macroscopic enlargement, hydronephrosis scores and changes in the histopathology of the tissue. These findings reflect the unresolved etiology of hydronephrosis in the ipsilateral kidney despite FCC treatment.

However, the primary focus of the present study was to evaluate the ability of FCC to preserve the function of the contralateral kidney not subjected to UUO treatment. Following UUO treatment, the contralateral normal kidney gradually loses function as its filtration workload is increased to compensate for the obstructed side. This compensatory hyperfiltration initially preserves waste clearance but eventually induces glomerular hypertension and nephron injury (Zhang *et al.,* 2024), driven by elevated renal perfusion pressure and associated biochemical and cellular changes (Gadelkareem *et al.,* 2022).

Results of the present study revealed that for the contralateral left kidney, the macroscopic size, tubular injury, inflammation, fibrosis and hydronephrosis scores were significantly reduced following FCC treatment (group G3) compared to UUO group without FCC treatment (group G2) and were comparable to those of the control group G1. Moreover, for the left kidney, the immuno-expression levels in the untreated UUO group G2 were higher compared with sham-operated control (G1) and the UUO+FCC-treated group (G3), specifically exhibiting increased immuno-expression of NGAL, SPP1 and TNF-α. These results are supported by those of the previous studies by Wasilewska *et al.* (2011) and Yang *et al.* (2024), who found a significant increase of NGAL in hydronephrosis patients, and suggested that NGAL can be used as a new biomarker for obstructive nephropathy. Furthermore, levels of NGAL, SPP1 and TNF-α biomarkers decreased in UUO+FCC-treated group compared to untreated UUO group, but were still higher compared to the Sham-operated control group.

For the left kidney, increased claudin-1 expression in UUO induced rats of group G2 indicated an early failure of the glomerular filtration barrier and showed a strong link to a decrease in GFR. The simultaneous elevation of claudin-1 and TNF-α indicated persistent inflammatory and fibrotic processes, aligning with the pathological characteristics associated with Alport-like nephropathy (Iida *et al.,* 2022). Elevated immunoreactivity of SPP1 and NGAL corroborated the existence of active inflammation and fibrosis, which were histologically manifested by interstitial matrix enlargement and significant renal hypertrophy (Jayne *et al.,* 2025). These pathological alterations were associated with increases in overall blood pressures, oedema of the lower limb, elevated cystatin C and SDMA levels, and decreased creatinine clearance (Xie *et al.,* 2022).

Conversely, FCC-treated rats undergoing UUO (group G3) displayed contralateral (left) renal morphology (length, width, thickness, volume and weight) similar to that of the sham group (G1). The ultrasonographic observations (length and hydronephrosis score) and histological scores (injury, inflammation and fibrosis) for the left kidney in group G3 closely resembled those in rats of control group G1, demonstrating that FCC efficiently maintained contralateral renal structure and function despite the stress generated by UUO. This renoprotective effect of FCC for the contralateral kidney is supported by the findings of Baris *et al.* (2023), who showed that choline and citicoline mitigate kidney injury while preserving renal architecture.

Renoprotective effects of FCC were further evidenced by suppression of NGAL, SPP1, and TNF-α immunoreactivity in UUO+FCC group G3 compared to UUO group G2. A previous study by Hasson *et al.* (2022) indicated that lower NGAL levels suggest interruption of the inflammation–fibrosis cycle, which is essential to be used as a novel hydronephrosis therapy. Reducing SPP1 and TNF-α expression levels are likely involved in curtailing fibroblast activation and extracellular matrix synthesis (Bonnard *et al.,* 2021), while anti-apoptotic action of SPP1 promoted tubular cell survival (Ding *et al.,* 2024).

Regarding mechanism, FCC serves as an antioxidant, attenuating TNF-α–driven inflammation. However, claudin-1 expression remained unchanged in group G3 (UUO+FCC) compared to G2 (UUO), which is consistent with the findings of Rowley *et al.* (2010) that choline does not directly inhibit claudin-1. Rather, it modulates claudin-1 indirectly through TGF-β suppression (Wang *et al.,* 2020). Unfortunately, the TGF-β and its correlation to claudin-1 levels could not be investigated in the present study.

Treatment success in rats of group G3 was corroborated by clinical markers, reduced SDMA, improved creatinine clearance (though still above control group G1), reduced cystatin C, and diminished peripheral oedema compared to rats of UUO group G2. Enhanced GFR likely prevented fluid accumulation, hinting at an osmotic diuretic effect of FCC. Mendoza-Martínez *et al.* (2022) reported that high choline promoted diuresis in dogs with urinary retention. According to Burri *et al.* (2019), dietary choline in dogs increased plasma choline concentrations, exhibited its beneficial effects on immune system and alleviated kidney disease.

Choline in FCC is oxidized and converted to betaine in renal cells, safeguarding cells from oxidative stress, aids in osmotic management and promotes water reabsorption. High choline intake may lower chronic kidney disease (CKD) risk by supporting osmoregulation, reducing oxidative damage, maintaining membrane integrity, lowering uric acid (Li *et al.,* 2024), and exerting anti-inflammatory effects (Kusuda *et al.,* 2020). According to Prakoso *et al.* (2025), choline present in FCC decreased COX-2 activity, resulting in reduced oxidative stress and enhanced endogenous antioxidant capacity in rats. Concurrently, Wang *et al.* (2023) underscored the significance of choline as a precursor to phosphatidylcholine, essential for preserving cellular membrane integrity. Herbal choline supplementation has been shown to enhance glomerular filtration rate and decrease hyperuricemia (Lin *et al.,* 2024), with an inverse relationship between dietary choline intake and the risk of chronic kidney disease (Jieru *et al.*, 2024), whereas inadequate choline intake worsened diabetic nephropathy (Al-Humadi *et al.,* 2025).

Despite these beneficial effects, choline can be metabolized by gut microbiota and the liver into trimethylamine-N-oxide (TMAO), a compound that increases cardiovascular risk in CKD patients (Zhou *et al.,* 2023). Taken together, these findings suggest that choline from FCC may have both beneficial (renal protection) and potentially harmful (TMAO-mediated cardiovascular risk) effects. One appears to support renal repair during UUO, while the other reflects systemic consequences arising from TMAO formation. Given this possibility, targeted preclinical studies are needed to determine the duration of FCC exposure than may influence both the likelihood of TMAO production and the pathways by which it is generated. Moreover, future studies should evaluate FCC in additional animal models combining renal and cardiac dysfunction, measure plasma and urinary TMAO levels to gauge cardiovascular implications, quantify TGF-β signalling to clarify its role in claudin-1 regulation and barrier integrity, and conduct dose–response experiments to identify the optimal therapeutic window that maximizes renal protection while minimizing adverse effects of FCC.

Conclusions: In conclusion, FCC treatment demonstrated robust renoprotective effects on the contralateral normal kidney in UUO rat models by preserving renal morphology and suppressing pro-inflammatory and pro-fibrotic markers (NGAL, SPP1, TNF-α). Systemic evaluation also indicated that FCC treatment improved renal function by decreased level of SDMA, stabilized cystatin C, and elevated creatinine clearance. Nevertheless, because choline can be metabolized into TMAO, the comprehensive safety and toxicity assessments are needed to be evaluated.

Ethical approval: The experimental procedures conducted in this study was reviewed and approved by the Ethical Clearance Committee of the Faculty of Veterinary Medicine, University of Wijaya Kusuma Surabaya, Indonesia (approval No. 225–KKE/IV/2025). This study was carried out in the Laboratory of Pharmacology, Faculty of Veterinary Medicine, University of Wijaya Kusuma Surabaya, Indonesia, during the period from January to August, 2025.

Funding: We gratefully acknowledge the financial support provided by the Indonesian Ministry of Higher Education, Science and Technology via the Indonesian Endowment Fund for Education (LPDP) under the EQUITY Program 2025 (Contract Number: 4301/B3/DT.03.08/2025 and 10107/UN1.P/Dit-Keu/HK.08.00/2025).

Acknowledgments: We are sincerely thankful to the staff of the Laboratory of Pharmacology, University of Wijaya, Kusuma Surabaya, Indonesia for their invaluable help throughout this study.

Competing interests: The author declare that they have no competing interests.

Authors contribution: YAP supervised the study, while the idea was conceptualized by YAP, ADW, ABAK, OMP, SW, PP and IPH. Experimental procedures were carried out by YAP, ADW, ABAK and OMP, while clinicopathological analysis was performed by SW and PP. Ultrasonography was done by IPH, while YAP, ADW, ABAK, OMP, SW, PP and IPH carried out writing of the draft, revising and approval of final manuscript.

Data availability: The datasets supporting the findings of this study are available within the article.

Generative AI Statement: The authors declare that no Gen AI/DeepSeek was used in the writing/creation of this manuscript.

REFERENCES

Al-Humadi AW, le Roux CW, Docherty NG *et al.,* 2025. Dietary choline deprivation exacerbates kidney injury in streptozotocin-induced diabetes in adult rats. Diabetology 6(1):8.

Arifianto D, Adji D, Sutrisno B, *et al.,* 2020. Renal histopathology, blood urea nitrogen and creatinine level of rats with unilateral ureteral obstruction. Indonesian Journal of Veterinary Sciences 1(1):1-9.

Baris E, Simsek O, Arici MA, *et al.,* 2023. Choline and citicoline ameliorate oxidative stress in acute kidney injury in rats. Bratislava Medical Journal 124(1):47–52.

Benoit SW, Ciccia EA and Devarajan P, 2020. Cystatin C as a biomarker of chronic kidney disease: latest developments. Expert Review of Molecular Diagnostics 20(10):1019–26.

Bombiński P, Brzewski M, Warchol S, *et al.,* 2018. Influence of diuretic (furosemide) on contrast medium distribution in computed tomography urography of high-grade hydronephrosis in children. Central European Journal of Urology 71(4):476–80.

Bonnard B, Martínez-Martínez E, Fernández-Celis A, *et al.,* 2021. Antifibrotic effect of novel neutrophil gelatinase-associated lipocalin inhibitors in cardiac and renal disease models. Scientific Reports 11(1):2591.

Burri L, Heggen K, and Storsve AB, 2019. Phosphatidylcholine from krill increases plasma choline and its metabolites in dogs. Veterinary World 12(5):671–76.

Chen S and Chiaramonte R, 2019. Estimating creatinine clearance in the nonsteady state: The determination and role of the true average creatinine concentration. Kidney Medicine 1(4):207–16.

Damian FB, de Almeida FK, Fernandes FS, *et al.,* 2022. Impact of hydronephrosis and kidney function on survival in newly diagnosed advanced cervical cancer. Gynecologic Oncology Reports 39:100934.

Dias AGF, Santin API, Brasileiro JCL, *et al.,* 2023. Effects of herbal choline as a replacement for choline chloride on myopathy, locomotor system, and hepatic health of broilers. Revista Brasileira de Zootecnia 52: e20220177.

Dilken O, Ince C, Kapucu A, *et al.,* 2023. Furosemide exacerbated the impairment of renal function, oxygenation and medullary damage in a rat model of renal ischemia/reperfusion induced AKI. Intensive Care Medicine Experimental 11(1):25.

Ding H, Xu Z, Lu Y, *et al.,* 2024. Kidney fibrosis molecular mechanisms Spp1 influences fibroblast activity through transforming growth factor beta smad signaling. iScience 27(9):109839.

Gadelkareem RA, Abdelraouf AM, El-Taher AM, *et al.,* 2022. Acute kidney injury due to bilateral malignant ureteral obstruction: Is there an optimal mode of drainage? World Journal of Nephrology 11(6):146–63.

Gasparis AP, Kim PS, Dean SM, *et al.,* 2020. Diagnostic approach to lower limb oedema. Phlebology 35(9):650–55.

Hasson DC, Watanabe-Chailland M, Romick-Rosendale L, *et al.,* 2022. Choline supplementation attenuates experimental sepsis-associated acute kidney injury. American Journal of Physiology-Renal Physiology 323(3): F255–F271.

He GD, Liu XC, Lu AS, *et al.,* 2022. Association of choline intake with blood pressure and effects of its microbiota-dependent metabolite trimethylamine-n-oxide on hypertension. Cardiovascular Therapeutics 2022:9512401.

Hidayah JH, Prakoso YA and Widyarini S, 2023. Brain histopathological changes after treatment using calabash fruit (*Crescentia cujete* L.) in rat model with artificially induced ischemic stroke. Advances in Animal and Veterinary Sciences 11(12):2003–2009.

Hosny M, Chan K, Ibrahim M, *et al.,* 2024. The management of symptomatic hydronephrosis in pregnancy. Cureus 16(1): e52146.

Iida M, Ohtomo S, Wada NA, *et al.,* 2022. TNF-α induces Claudin-1 expression in renal tubules in Alport mice. PLoS One 17(3): e0265081.

Ilgi M, Sr Bayar G, Abdullayev E, *et al.,* 2020. Rare causes of hydronephrosis in adults and diagnosis algorithm: analysis of 100 cases during 15 years. Cureus 12(5): e8226.

Isac GV and Ionescu NS, 2025. Predictive factors for spontaneous resolution in primary obstructive megaureter: the impact of hydronephrosis severity on clinical outcomes. Journal of Clinical Medicine 14(7):2463.

Jayne D, Herbert C, Anquetil V, *et al.,* 2025. Exploring the critical role of tight junction proteins in kidney disease pathogenesis. Nephron 149(4):240–250.

Jieru P, Zhang S, Cai L, *et al.,* 2024. Dietary choline intake and health outcomes in U.S. adults: exploring the impact on cardiovascular disease, cancer prevalence, and all-cause mortality. Journal of Health, Population and Nutrition 43(1):59.

Jo CH, Kim S and Kim GH, 2022. Claudins in kidney health and disease. Kidney Research and Clinical Practice 41(3):275–87.

Kenny TC, Scharenberg S, Abu-Remaileh M, *et al.,* 2025. Cellular and organismal function of choline metabolism. Nature Metabolism 7(1):35–52.

Kobori H, Mori H, Masaki T, *et al.,* 2013. Angiotensin II blockade and renal protection. Current Pharmaceutical Design 19(17):3033–42.

Kusuda R, Carreira EU, Ulloa L, *et al.,* 2020. Choline attenuates inflammatory hyperalgesia activating nitric oxide/cGMP/ATP-sensitive potassium channels pathway. Brain Research 1727:146567.

Li C, Li J, Diao Z, *et al.,* 2024. Associations of dietary choline intake and kidney function with hyperuricemia in Chinese children and adolescents: a cross-sectional study. EClinicalMedicine 79(6):103012.

Lin Z, Gupta JK, Maqbool M, *et al.,* 2024. The therapeutic management of chemical and herbal medications on uric acid levels and gout: modern and traditional wisdom. Pharmaceuticals 17(11):1507.

Liu JJ, Liu S, Gurung RL, *et al.,* 2025. Urine choline oxidation metabolites predict chronic kidney disease progression in patients with type 2 diabetes. The Journal of Clinical Endocrinology and Metabolism 111(1): e225-e233.

Ma ZY, Zhang XF, Hu YZ, *et al.,* 2024. Comparison of staining quality between rapid and routine hematoxylin and eosin staining of frozen breast tissue sections: An observational study. Journal of International Medical Research 52(6):3000605241259682. doi: 10.1177/03000605241259682.

Mendoza-Martínez GD, Hernández-García PA, Plata-Pérez FX, *et al.,* 2022. Influence of a polyherbal choline source in dogs: body weight changes, blood metabolites, and gene expression. Animals 12(10):1313.

Napitupulu T, Hardja Y, Susanto M, *et al.,* 2023. Correlation between the grade of hydronephrosis with surgical outcomes after ultrasound-guided supine percutaneous nephrolithotomy: A retrospective observational study. Medeniyet Medical Journal 38(2):120–27.

Patel RV, Johal N, Evans K, *et al.,* 2014. Antenatal mild hydronephrosis with subsequent polyp of the upper ureter in a child presenting with recurrent Dietl's crisis. BMJ Case Reports 2014: bcr2013202967. doi: 10.1136/bcr-2013-202967.

Pérez-Aizpurua X, Cabello Benavente R, Bueno Serrano G, *et al.,* 2024. Obstructive uropathy: Overview of the pathogenesis, etiology and management of a prevalent cause of acute kidney injury. World Journal of Nephrology 13(2):93322.

Pokrovskaya A, Vetluzhskaya M, Bazhanova U, *et al.,* 2021. Rare cause of asymptomatic giant hydronephrosis. BMJ Case Reports 14(3): e241357. doi: 10.1136/bcr-2020-241357.

Prakoso YA, Susilo A and Widyarini S, 2024. The standardization and efficacy of fermented *Crescentia cujete* (L.) in combination with enrofloxacin against artificially induced pneumonic pasteurellosis in rat models. Open Veterinary Journal 14(12):3404–3416.

Prakoso YA, Isla KJV and Wijayanti AD, 2025. Effects of repeated 14-day oral toxicity of fermented *Crescentia cujete* (L.) on histopathology, GM-CSF, COX-2, antioxidants, and MDA levels in male *SPrague Dawley* rats. Open Veterinary Journal 15(12):6527-40.

Rowley TJ, McKinstry A, Greenidge E, *et al.,* 2010. Antinociceptive and anti-inflammatory effects of choline in a mouse model of postoperative pain. British Journal of Anaesthesia 105(2):201-207.

Shi Y and Zhu R, 2023. Analysis of damage-associated molecular patterns in amyotrophic lateral sclerosis based on ScRNA-seq and bulk RNA-seq data. Frontiers in Neuroscience 17:1259742.

Vilskersts R, Vilks K, Videja M, *et al.,* 2020. Rats with congenital hydronephrosis show increased susceptibility to renal ischemia-reperfusion injury. Physiological Reports 8(22): e14638.

Wang K, Pascal LE, Li F, *et al.,* 2020. Tight junction protein claudin-1 is downregulated by TGF-β1 via MEK signaling in benign prostatic epithelial cells. Prostate 80(14):1203–15.

Wang YN, Zhang ZH, Liu HJ, *et al.,* 2023. Integrative phosphatidylcholine metabolism through phospholipase A_2 in rats with chronic kidney disease. Acta Pharmacologica Sinica 44(2):393–405.

Wasilewska A, Taranta-Janusz K, Dębek W, *et al.,* 2011. KIM-1 and NGAL: new markers of obstructive nephropathy. Pediatric Nephrology 26(4):579–86.

Wijayanti AD, Prakoso YA, and Isla KJV, 2024. Effects of fermented *Crescentia cujete* L. on the profile of hematology, clinical chemistry, and circulatory CD4+/CD8+ in Sprague Dawley rats. Open Veterinary Journal 14(9):2475–83.

Wilujeng S, Prakoso YA and Wirjaatmadja R, 2023. Effects of extraction, fermentation, and storage processes on the level of choline derived from calabash fruit (*Crescentia cujete* L.). Journal of Research in Pharmacy 27(2):620–26.

Xie T, Zhou H, Gao Y, *et al.,* 2022. Serum and urinary neutrophil gelatinase-associated lipocalin levels as early markers of the renal function in patients with urinary stone-induced hydronephrosis. Frontiers in Surgery 9:843098.

Yang L, Wu L, Pu J, *et al.,* 2024. The diagnostic accuracy of urinary neutrophil gelatinase-associated lipocalin in assessing kidney function in severe hydronephrosis. Translational Andrology and Urology 13(8):1555–65.

Yaxley J and Yaxley W, 2023. Obstructive uropathy - acute and chronic medical management. World Journal of Nephrology 12(1):1–9.

Zhang L, Mo X, Jiang Z, *et al.,* 2024. Contralateral renal change in a unilateral ureteral obstruction rat model using intravoxel incoherent motion diffusion-weighted imaging. Renal Failure 46(2):2359642.

Zhou R, Yang M, Yue C, *et al.,* 2023. Association between dietary choline intake and cardiovascular diseases: national health and nutrition examination survey 2011-2016. Nutrients 15(18):4036.